

## Precuneal gliomas promote behaviorally relevant remodeling of the functional connectome

Sam Ng, MD,<sup>1,2</sup> Jeremy Deverdun, PhD,<sup>3,4</sup> Anne-Laure Lemaître, PhD,<sup>1,2</sup> Davide Giampiccolo, MD,<sup>5-7</sup> Emmanuelle Le Bars, PhD,<sup>3,4</sup> Sylvie Moritz-Gasser, PhD,<sup>1,2</sup> Nicolas Menjot de Champfleury, MD, PhD,<sup>3,4</sup> Hugues Duffau, MD, PhD,<sup>1,2</sup> and Guillaume Herbet, PhD<sup>1,2</sup>

Departments of <sup>1</sup>Neurosurgery and <sup>4</sup>Neuroradiology, Gui de Chauliac Hospital, Montpellier University Medical Center, Montpellier; <sup>2</sup>Team “Neuroplasticity, Stem Cells and Low-grade Gliomas,” Institute of Functional Genomics of Montpellier, University of Montpellier, CNRS, INSERM, Montpellier; <sup>3</sup>I2FH, Institut d’Imagerie Fonctionnelle Humaine, Gui de Chauliac Hospital, Montpellier University Medical Center, Montpellier, France; <sup>5</sup>Department of Clinical and Experimental Epilepsy, UCL Queen Square Institute of Neurology, University College London; <sup>6</sup>Victor Horsley Department of Neurosurgery, National Hospital for Neurology and Neurosurgery, Queen Square, London; and <sup>7</sup>Department of Neurosurgery, Institute of Neurosciences, Cleveland Clinic London, United Kingdom

**OBJECTIVE** The precuneus hosts one of the most complex patterns of functional connectivity in the human brain. However, due to the extreme rarity of neurological lesions specifically targeting this structure, it remains unknown how focal damage to the precuneus may impact resting-state functional connectivity (rsFC) at the brainwide level. The aim of this study was to investigate glioma-induced rsFC modulations and to identify patterns of rsFC remodeling that accounted for the maintenance of cognitive performance after awake-guided surgical excision.

**METHODS** In a unique series of patients with *IDH1*-mutated low-grade gliomas (LGGs) infiltrating the precuneus who were treated at a single neurosurgical center (Montpellier University Medical Center, 2014–2021), the authors gauged the dynamic modulations induced by tumors on rsFC in comparison with healthy participants. All patients received a preoperative resting-state functional MRI and underwent operation guided by awake cognitive mapping. Connectome multivariate pattern analysis (MVPA), seed-network analysis, and graph theoretical analysis were conducted and correlated to executive neurocognitive scores (i.e., phonological and semantic fluencies, Trail-Making Test [TMT] parts A and B) obtained 3 months after surgery.

**RESULTS** Seventeen patients with focal precuneal infiltration were selected (mean age  $38.1 \pm 11.2$  years) and matched to 17 healthy participants (mean age  $40.5 \pm 10.4$  years) for rsFC analyses. All patients underwent awake cognitive mapping, allowing total resection ( $n = 3$ ) or subtotal resection ( $n = 14$ ), with a mean extent of resection of  $90.6\% \pm 7.3\%$ . Using MVPA (cluster threshold:  $p$ -false discovery rate corrected  $< 0.05$ , voxel threshold:  $p$ -uncorrected  $< 0.001$ ), remote hotspots with significant rsFC changes were identified, including both insulas, the anterior cingulate cortex, superior sensorimotor cortices, and both frontal eye fields. Further seed-network analyses captured 2 patterns of between-network redistribution especially involving hyperconnectivity between the salience, visual, and dorsal attentional networks. Finally, the global efficiency of the salience-visual-dorsal attentional networks was strongly and positively correlated to 3-month postsurgical scores ( $n = 15$ ) for phonological fluency ( $r_{15} = 0.74$ ,  $p = 0.0027$ ); TMT-A ( $r_{15} = 0.65$ ,  $p = 0.012$ ); TMT-B ( $r_{15} = 0.70$ ,  $p = 0.005$ ); and TMT-B-A ( $r_{15} = 0.62$ ,  $p = 0.018$ ).

**CONCLUSIONS** In patients with LGGs infiltrating the precuneus, remote and distributed functional connectivity modulations in the preoperative setting are associated with better maintenance of cognitive performance after surgery. These findings provide a new vision of the mechanistic principles underlying neural plasticity and cognitive compensation in patients with LGGs.

<https://thejns.org/doi/abs/10.3171/2022.9.JNS221723>

**KEYWORDS** precuneus; functional connectivity; neuroplasticity; executive function; low-grade glioma; awake surgery; oncology

**ABBREVIATIONS** BOLD = blood oxygen level–dependent; CC = clustering coefficient; DAN = dorsal attentional network; DMN = default-mode network; FDR = false discovery rate; FPN = frontal-parietal network; GE = global efficiency; LGG = low-grade glioma; MNI = Montreal Neurological Institute; MVPA = multivariate pattern analysis; ROI = region of interest; rsFC = resting-state functional connectivity; rsfMRI = resting-state functional MRI; TMT-A, TMT-B = Trail-Making Test parts A and B.

**SUBMITTED** July 25, 2022. **ACCEPTED** September 8, 2022.

**INCLUDE WHEN CITING** Published online October 28, 2022; DOI: 10.3171/2022.9.JNS221723.

**N**EUROLOGICAL lesions specifically targeting the human precuneus are rarely reported. This historically neglected quadrangular area, lodged in the medial face of the parietal lobe, has however drawn important attention over recent decades: it has been suggested as one of the most critical hubs of the human brain,<sup>1</sup> and a wide range of higher-order cognitive functions are presumably mediated by this parietal area, including self-directed cognition,<sup>2-4</sup> autobiographical memory,<sup>5</sup> and bodily awareness.<sup>6</sup> In particular, the inferior subregion of the precuneus, together with the adjacent posterior cingulate cortex, are pivotal areas of the default-mode network (DMN).<sup>7</sup> Furthermore, the precuneus hosts one of the most complex patterns of structural and functional connectivity, and is engaged in regulating functional connectivity between the main large-scale networks of the brain in a context-sensitive manner.<sup>8</sup>

In view of its high level of centrality, it is widely expected that focal precuneal damage may cause brainwide modulations of functional connectivity, as suggested by lesion modeling studies.<sup>9</sup> It is indeed established that lesions involving cortical hubs are capable not only of disrupting local networks but also of causing widespread, nonlocal impacts on functional architecture that may reflect either network dysfunction<sup>10</sup> or remote compensatory network reorganizations.<sup>11</sup> In the latter case, the ability of the brain to reshape its functional networks in response to an acute pathological condition has been pointed out as a plausible biological substrate of plasticity, potentially conditioning neurological recovery in stroke patients.<sup>12</sup> In this context, the extent to which well-circumscribed lesions of the precuneus might induce remote redistribution of between-network functional connectivity and how these modulations might be behaviorally relevant remain to be elucidated.

Over different lesion models, slowly infiltrating brain tumors (especially low-grade gliomas [LGGs]) are the most established entities to study the potential of the brain to develop lesion-induced compensatory mechanisms. The slow-growth kinetics of LGGs makes it indeed possible to perform extensive surgical removal<sup>13</sup> with only limited neuropsychological consequences thanks to modern awake mapping techniques,<sup>14</sup> because functional networks have the potential to progressively reorganize in parallel to the tumoral expansion. Previous studies focusing on gliomas have suggested distant alterations of functional connectivity,<sup>15</sup> along with strong homotopic functional reshaping,<sup>16</sup> but the brainwide redistribution of functional connectivity following tumor infiltration has not been investigated, especially in the context of lesions targeting such a highly integrative cortical hub as the precuneus.

Here we used neuroimaging data from a unique series of 17 patients with an LGG infiltrating the precuneus. Our primary objective was to capture the modulations of resting-state functional connectivity (rsFC) induced by tumors. We observed specific between-network schemes of hyperconnectivity in comparison to healthy participants. We further showed that the global topological organization of the patients' modulated networks was a strong predictor of cognitive resilience after surgical excision. Overall, the current study suggests that precuneal dam-

age promotes distributed patterns of rsFC compensation as markers of neural plasticity.

## Methods

### Study Design and Participants

We retrospectively screened patients admitted to our institution between January 2014 and January 2021 for an LGG located within the precuneus. Only patients with available preoperative resting-state functional MRI (rsfMRI) were included. In order to select homogeneous tumors with similar growth kinetics and thus with comparable impact on rsFC measures,<sup>15</sup> we retained only LGGs whose histomolecular profile was further confirmed with an *IDH1*-mutated status. Other exclusion criteria were previous oncological treatments (e.g., resection, chemotherapy, or brain radiation) and brain midline shift due to tumor mass effect. Overall, 17 patients were included (mean age  $38.1 \pm 11.2$  years) and were matched to 17 healthy subjects (mean age  $40.5 \pm 10.4$  years).

### Standard Protocol Approvals, Registrations, and Patient Consents

This study was conducted in compliance with the ethics standards of our National College Institution for a retrospective study. All patients gave informed consent to the retrospective extraction of clinical and imaging data from their medical records. All healthy control participants also provided written consent.

### Neuroimaging Acquisition

Structural and functional imaging sequences were acquired with a 1.5T (Avanto) or a 3T (Skyra) MRI scanner (Siemens), using a 32-channel head coil, as part of the patients' care protocol. To account for its potential effects on rsFC, we used between-scanner difference as a nuisance covariate in the analyses.<sup>16</sup>

For this study we used the following modalities. 1) 3D MPRAGE T1-weighted images with the following parameters (1.5T/3T): TR 1880/1700 msec, TE 3.4/2.5 msec, TI 1100/922 msec, field of view  $256 \times 256$  mm, voxel size  $1 \times 1 \times 1$  mm<sup>3</sup>, 176 axial slices, and flip angle  $15^\circ/9^\circ$ . 2) rsfMRI T2\*-weighted gradient echo-echo planar imaging with the following parameters (1.5T/3T): TR 2320/2400 msec, TE 50/30 msec, voxel size  $3 \times 3 \times 5.5/2.39 \times 2.39 \times 3$  mm<sup>3</sup>, 28/39 interleaved slices, 200 whole-brain volumes, flip angle  $90^\circ$ , duration 8.07 minutes. For rsfMRI, participants were asked to remain still with eyes closed and to let their minds wander freely. 3) FLAIR images.

Note that all tumor volumes were based on FLAIR images, obtained on the preoperative and on the 3-month postoperative imaging sessions, using a dedicated software program (Myrian; Intracase).

### Surgical Procedure

All patients included in this study underwent a tumor resection in the 72 hours following rsfMRI acquisition. An asleep-awake-asleep protocol was performed in all cases by using electrostimulation mapping, as extensively described elsewhere.<sup>17</sup> All surgical procedures were

performed by the same surgeon (H.D.). A bipolar probe (NIMBUS stimulator; Newmedic France) with 5-mm spacing, 60-Hz biphasic electrostimulation, and current intensities ranging from 1.5 to 5 mA was used for both cortical and subcortical electrostimulation. Intraoperative mapping included motor and somatosensory monitoring, combined with speech fluencies, denomination task, image-association task, line bisection task, face-based mentalizing task, and constant dual-tasking monitoring. In all cases surgical excision was based on functional responses, obtained at both the cortical and the subcortical levels.

### Neuropsychological Data

Patients were administered selected neuropsychological tasks appraising aspects of executive functioning at 3 months after surgery as part of their routine clinical management—these included phonological fluencies;<sup>18</sup> semantic fluencies;<sup>18</sup> and parts A, B, and B-A of the Trail-Making Test (TMT).<sup>19</sup> Participants' scores were appropriately aligned to published normative data (considering age, sex, and educational level) and converted into z-scores using the French GREFEX normative data sets.<sup>20</sup> Note that neuropsychological evaluations were not administered systematically before surgery in routine clinical practice at the time of acquisition. Thus, it was not possible to compute further correlation analyses involving preoperative neurocognitive performance.

### Functional Image Processing and Functional Data Analysis

Image processing was performed with MATLAB (Release 2018b; The MathWorks, Inc.), SPM12 (www.fil.ion.ucl.ac.uk/spm/software/spm12), and the Conn toolbox<sup>21</sup> (version 20.b, www.nitrc.org/projects/conn). The default preprocessing and denoising pipeline were applied, including functional realignment and unwarping, slice-timing and motion correction, segmentation, normalization to Montreal Neurological Institute (MNI) space, smoothing of functional data set (8-mm full width at half maximum gaussian kernel), temporal bandpass filtering (0.008–0.09 Hz), and linear detrending. No tumor masking was applied during the registration process, but each normalized image was systematically and carefully checked to exclude potentially inaccurate registrations. Of note, we selected only infiltrative LGGs without associated mass effect or anatomical deformation.<sup>16,22</sup>

Using anatomical component-based noise reduction (aCompCor), noise components from white matter and cerebrospinal areas were controlled by estimating 5 orthogonal time series and their derivatives within each area. Twelve additional potential noise factors were defined from the estimated subject-motion parameters in order to minimize motion-related blood oxygen level-dependent (BOLD) signal variability. Factors identified as having potential confounding effects on the BOLD signal were estimated and removed separately for each voxel and for each subject by using ordinary least squares regression. Scrubbing was used to remove outlier volumes, defined as framewise displacement of more than 0.9 mm from the previous frame or global BOLD signal change of more

than 5 SDs.<sup>23</sup> Runs were excluded from analyses if more than 20% of the acquired volumes were scrubbed (no runs met this cutoff). The number of scrubbed volumes was similar between groups (see Supplementary Fig. 1). All rsFC measures (see below) were processed through a general linear model. Bivariate correlation coefficients were converted to normalized z-scores by using Fisher's transform to allow subsequent general linear model analyses. One-way ANCOVA or MANCOVA studies were then performed to investigate potential differences between patients with a precuneal lesion ( $n = 17$ ) and healthy controls ( $n = 17$ ), systematically including age, sex, handedness, and scanner type as nuisance covariates. Given the expected symmetry of rsFC of the precuneus through the right and left cerebral hemispheres,<sup>24</sup> patients with right precuneal lesions ( $n = 11$ ) and left precuneal lesions ( $n = 6$ ) were grouped together to increase statistical power.

### Precuneal Connectivity Analysis

To investigate rsFC changes between the precuneus and all other voxels within the brain, we used the precuneus parcellation of the FSL Harvard-Oxford atlas as a seed region of interest (ROI) to generate ROI<sub>precuneus</sub>-to-voxel connection maps. Of note, this parcellation covers both right and left precuneus regions. Significant differences between groups were selected using cluster-level inferences in voxel-based analyses (cluster threshold:  $p$ -false discovery rate [FDR] corrected  $< 0.05$ ; voxel threshold:  $p$ -uncorrected  $< 0.001$ ), as recommended.<sup>25</sup>

### Multivariate Pattern Analysis

Next, to mitigate the effects of user selection bias through the practice of a priori ROI selection, we used a data-driven approach in which connectome multivariate pattern analysis (MVPA) was used. MVPA is a whole-brain voxel-to-voxel approach which has now been well validated;<sup>21,26</sup> the method computes connectivity between residualized BOLD time series in a given voxel and all other voxels in the brain; it iterates this process voxelwise across the brain. By using principal components analysis, the dimensionality of the data is reduced to 64 spatial components. Following convention,<sup>26,27</sup> we retained the first 4 of these 64 components to yield MVPA-derived maps (i.e., representing an approximate ratio of 1:10 to 1:5 between the number of components extracted and the number of participants analyzed). The percent of variance of rsFC explained by the first 4 principal components was 82.8%, which is in line with previous reports.<sup>26</sup> Then, MANCOVAs were conducted with each participant's 4 factor scores at each voxel as dependent variables. Significant differences were selected using cluster-level inferences (cluster threshold:  $p$ -FDR corrected  $< 0.05$ ; voxel threshold:  $p$ -uncorrected  $< 0.001$ ), as previously recommended.<sup>25</sup> Next, assuming that supratentorial suprathreshold clusters identified with MVPA (ROI<sub>MVPA</sub>) might unveil critical loci of connectivity change, we generated ROI<sub>MVPA</sub>-to-voxel connection maps, as proposed in previous studies.<sup>27,28</sup>

### Network Analysis

Then, we were interested in exploring the possible in-

**TABLE 1. Main clinical and radiological features in 17 patients with LGGs**

Case No.	Age (yrs)	Sex	Handedness	Educational Level (yrs)	Tumor Side	Preop Vol (cm <sup>3</sup> )*	Postop Vol (cm <sup>3</sup> )*
1	34	M	Rt	11	Rt	12.5	2.0
2	48	M	Rt	17	Rt	6.4	1.0
3	38	M	Rt	14	Rt	23.2	0.0
4	41	F	Rt	16	Rt	28.6	5.0
5	23	F	Rt	12	Rt	106.6	1.0
6	40	F	Rt	14	Rt	26.9	6.0
7	32	F	Rt	17	Rt	30.1	2.0
8	43	F	Rt	14	Rt	12.3	0.5
9	18	M	Rt	NR	Rt	13.8	0.0
10	46	F	Rt	15	Rt	5.8	0.5
11	29	M	Rt	17	Rt	34.5	7.0
12	52	M	Lt	17	Lt	44.7	6.0
13	36	F	Rt	15	Lt	17.9	1.0
14	26	F	Rt	17	Lt	27.4	0.0
15	52	M	Rt	14	Lt	67.4	9.0
16	55	M	Rt	14	Lt	7.3	0.5
17	39	F	Lt	15	Lt	44.1	4.0

NR = not reported.

\* Tumor volume based on FLAIR infiltration measures.

teractions between ROI<sub>MVPA</sub> and the main functional hubs belonging to the established canonical networks. These 7 supratentorial functional networks (i.e., DMN, sensorimotor network, visual network, salience network, dorsal attentional network [DAN], frontal-parietal network [FPN], and language network) were defined from Conn independent component analyses of 497 subjects belonging to the Human Connectome Project data set. To this end, we compared ROI<sub>MVPA</sub>-to-network connections between groups by computing an ROI-to-ROI analysis, using multivariate parametric statistics with recommended thresholding<sup>29</sup> (cluster threshold: p-FDR corrected < 0.05; connection threshold: p-uncorrected < 0.05). A data-driven clustering algorithm<sup>30</sup> was used so that ROI<sub>MVPA</sub> were grouped and sorted within canonical networks according to the similarity of their functional connectivity.

### Graph Theory Analyses

In an additional line of analyses, we used graph theory to gauge the global efficiency (GE) and the clustering coefficient (CC) of the main canonical networks showing significant schemes of hyperconnectivity in response to tumor infiltration. GE is often used as a measure of “the overall capacity for parallel information transfer and integrated processing.”<sup>31</sup> CC is known as an index of segregation (or specialization) of a given nodal connectivity.<sup>31</sup> Both GE and CC were previously reported as behaviorally relevant measures in pathological conditions.<sup>32,33</sup> Details about the computation of graph theoretical measures are provided in Supplementary Methods. We further assessed the hypothesis that topological measures of redistributed networks could be associated with cognitive performance after surgery. Adjusting for age, nonparametric Spearman partial correlation analyses between individual average

GE/CC values and postoperative neuropsychological z-scores (TMT-A, TMT-B, TMT-B-A, phonological fluency, and semantic fluency) were computed using RStudio version 2021.09.1 Build 372 (R Foundation; “ppcor” package version 1.1, <https://cran.r-project.org/web/packages/ppcor/ppcor.pdf>).

### Spatial Positioning of Positive Stimulation Sites

Stimulations eliciting cognitive responses during functional mapping were embedded in the MNI space, using operative reports, intraoperative photographs, and 3-month postoperative MRI. The 3D pial mesh models were generated using BrainVISA/Anatomist software (version 5.0, CEA I2BM; CATI Neuroimaging, INSERM IFR49 and CNRS), to enable an accurate positioning of each stimulation site. The following intraoperative responses were assessed, using intraoperative tasks: anarthria (disorders in producing speech), anomia (disorders in naming a picture), dystonic movements, movement arrests, somatosensory disorders, visual disorders, spatial neglect,<sup>34</sup> semantic association impairment,<sup>35</sup> mentalizing impairment,<sup>36</sup> and self-evaluation disorders.<sup>37</sup>

### Data Availability

Data are available upon request.

## Results

### Study Participants

Patients and healthy controls were comparable in terms of age (median 39 [range 18–55] vs 43 [range 24–58] years, respectively; Mann-Whitney U-test = 130, *p* = 0.63), sex (Fisher’s exact test, *p* = 0.73), and educational level (Mann-Whitney U-test = 95, *p* = 0.13). The main clinical

**TABLE 2. Neuropsychological scores in 17 patients with LGGs**

Case No.	Preop Phon Fluency	Postop Phon Fluency*	Preop Sem Fluency	Postop Sem Fluency*	Preop TMT-A	Postop TMT-A*	Preop TMT-B	Postop TMT-B*	Preop TMT-B-A	Postop TMT-B-A*
1	NA	-1.67	NA	-1.38	NA	-1.58	NA	-2.21	NA	-1.70
2	-1.70	0.84	-1.47	-2.16	NA	1.07	NA	0.88	NA	0.29
3	1.52	0.61	-0.15	0.83	1.08	0.25	1.04	0.77	NA	0.74
4	0.52	0.84	2.32	2.90	1.57	0.36	1.88	0.88	1.10	0.76
5	-1.36	-2.12	-0.88	-0.63	-0.75	-0.33	-0.95	-1.00	-0.63	-0.95
6	NA	NA	NA	NA	NA	NA	NA	NA	NA	NA
7	NA	-0.45	NA	0.22	NA	-0.17	NA	-0.14	NA	-0.05
8	NA	-0.11	NA	-1.01	NA	-1.29	NA	-1.79	NA	-1.19
9	NA	NA	NA	NA	NA	NA	NA	NA	NA	NA
10	-1.22	-0.59	-1.13	-1.81	0.21	0.36	0.38	-0.83	0.29	-1.19
11	0.76	0.61	0.59	0.34	1.16	1.42	1.31	0.91	0.79	0.16
12	0.84	1.16	1.63	-1.36	-1.29	-2.93	-0.46	-3.67	0.33	-2.24
13	-0.45	-1.21	-0.15	-1.37	1.08	-1.75	0.91	-2.05	0.37	-1.26
14	-0.91	0.30	0.95	1.80	0.83	0.42	1.09	0.32	0.74	0.11
15	-1.54	-0.75	-1.82	-3.66	-0.21	-9.07	-1.46	-9.46	-1.52	-4.76
16	-0.14	0.10	-0.90	0.63	0.57	-0.64	-0.88	-0.96	-1.38	-0.67
17	0.61	0.45	0.46	-1.49	0.41	-0.67	-0.14	-1.59	-0.42	-1.42

NA = not available; Phon = Phonological; Sem = Semantic.

All results are presented as z-scores, obtained from published normative data accounting for age, sex, and educational level.

\* At 3-month postoperative evaluation.

features are provided in Table 1. Neuropsychological data are displayed in Table 2. The tumor infiltration overlap map (n = 17) displayed in Fig. 1 indicates a homogeneous coverage of the precuneus extending to the posterior cingulate cortex.

**Surgical Data**

All patients underwent intraoperative awake cognitive

mapping. Three patients underwent total resections and 14 underwent subtotal resections (i.e., tumor residual < 10 cm<sup>3</sup> according to previous classifications<sup>38,39</sup>), with a mean extent of resection of 90.6% ± 7.3%.

**Intraoperative Mapping Results**

Overall, 162 positive stimulations were elicited, including 73 somatosensory disorders, 21 dystonic movements,

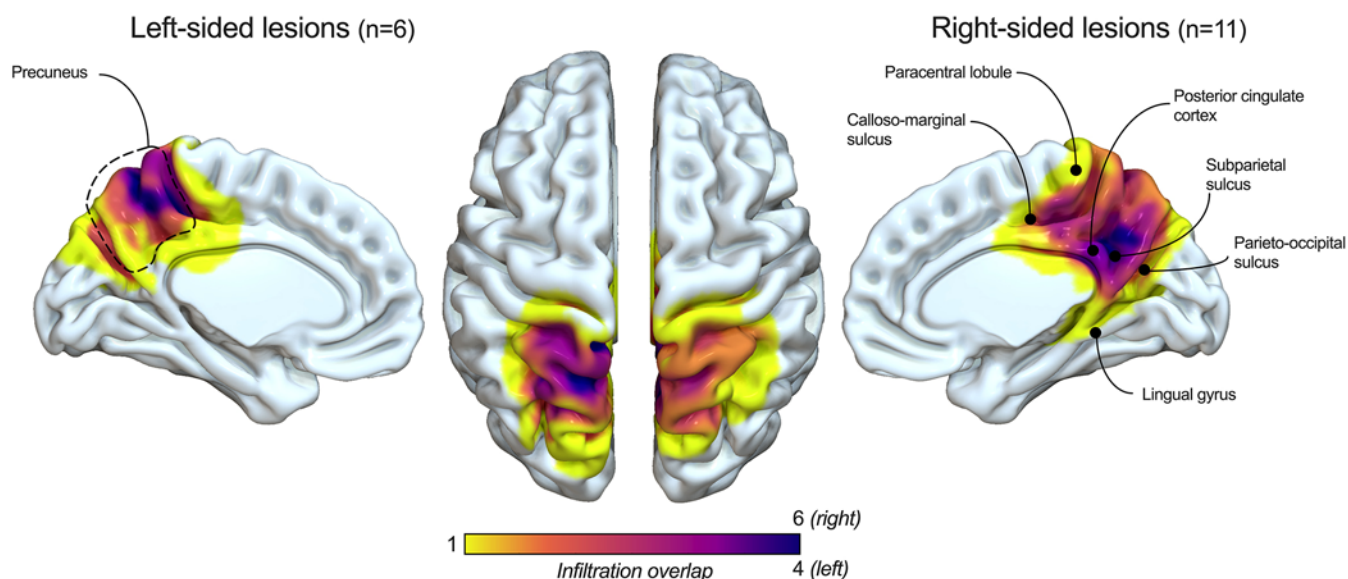


**FIG. 1.** Lesion overlap maps. Density overlap cortical map of left-sided lesions (n = 6) and right-sided lesions (n = 11). Color bar indicates lesion density. Figure is available in color online only.

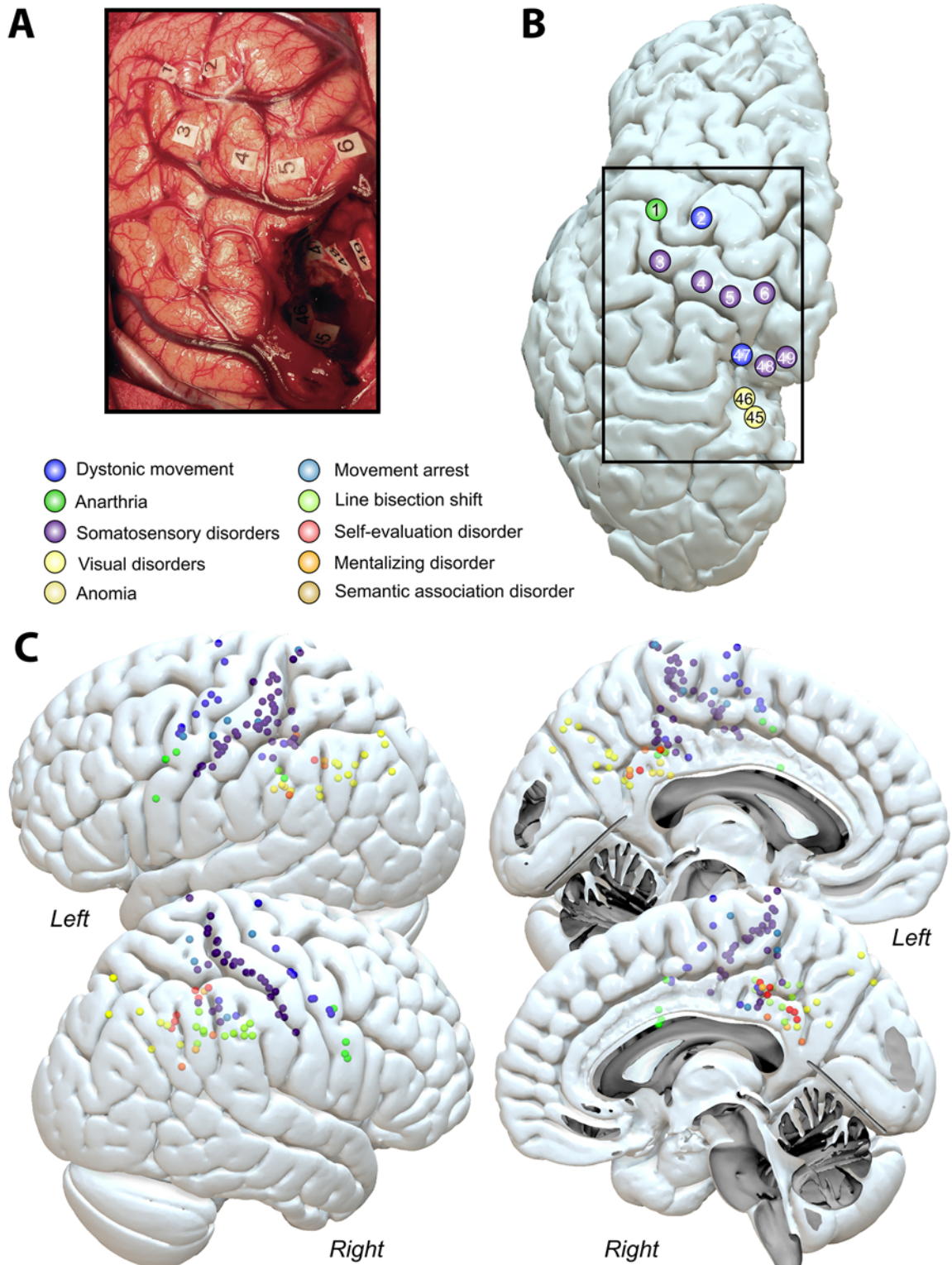


**FIG. 2.** Intraoperative mapping. **A:** Intraoperative photograph of a left precuneal resection. **B:** Pial reconstruction of the brain displayed in panel A and spatial positioning of unmasked stimulation sites. **C:** Positive stimulation sites (n = 162) obtained from cognitive electrostimulation mapping in the 17 patients with precuneal gliomas. Figure is available in color online only.

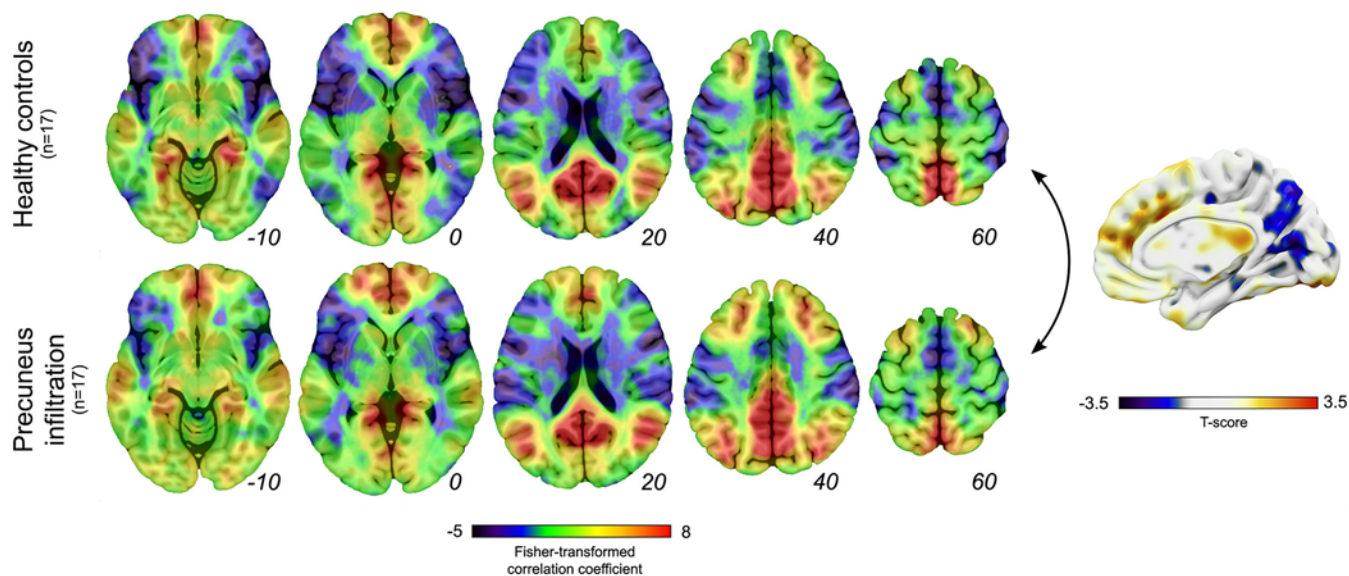


**FIG. 3.** Precuneus-to-voxel connectivity maps. Functional connectivity between the precuneus and all other voxels within the brain ( $ROI_{\text{precuneus}}$ -to-voxel connectivity maps) in healthy controls ( $n = 17$ ) and in patients with precuneal infiltration ( $n = 17$ ). The precuneus parcellation of the FSL Harvard-Oxford atlas was used as a seed. Significant differences between groups were selected using cluster-level inferences in voxel-based analyses (cluster threshold:  $p$ -FDR corrected  $< 0.05$ ; voxel threshold:  $p$ -uncorrected  $< 0.001$ ). Figure is available in color online only.

20 visual disorders, 12 spatial neglects, 9 movement arrests, 8 anarthrias, 7 disturbed self-evaluation processing, 5 semantic association disorders, 4 anomias, and 3 mentalizing impairments. An intraoperative photograph and an illustration of the intraoperative mapping are displayed in Fig. 2A and B, respectively. All stimulation sites are displayed in the MNI space in Fig. 2C.

### $ROI_{\text{precuneus}}$ -to-Voxel Analyses

The average  $ROI_{\text{precuneus}}$ -to-voxel connectivity maps in patients with tumors and healthy controls are reported in Fig. 3. A typical DMN pattern was identified in both patients and healthy subjects, without statistical difference between the 2 connectivity maps, suggesting that tumor-related precuneal infiltrations did not drastically impact the DMN intranetwork connectivity.

### $ROI_{\text{MVPA}}$ -to-Voxel and $ROI_{\text{MVPA}}$ -to-Network Analyses

Using connectome MVPA, we identified 6 symmetrical  $ROI_{\text{MVPA}}$  (i.e., ROIs with significant changes of functional connectivity between both groups), including the left and right insulas, the anterior cingulate cortex, left and right precentral and adjacent superior frontal gyri, and left and right paramedian postcentral gyri (Table 3 and Fig. 4).  $ROI_{\text{MVPA}}$ -to-voxel analyses indicated various upmodulations and some downmodulations of rsFC between  $ROI_{\text{MVPA}}$  and other brain areas (Fig. 4, left side of each panel; also, significant clusters are detailed in Supplementary Table 1).

In subsequent  $ROI_{\text{MVPA}}$ -to-network analyses (Fig. 4, right side of each panel), 2 distinct between-network hyperconnectivity patterns were identified: 1) a salience-visual-DAN pattern, and 2) a DAN-language-salience-FPN pattern.

### Graph Theory and Behavior Correlates

We assumed that the between-network modulations previously identified (namely, salience-visual-DAN and DAN-language-salience-FPN hyperconnectivity patterns) might be predictors of cognitive status after tumor resection. After controlling for age, the average GE of the salience-visual-DAN was strongly and positively correlated to 3-month postsurgical z-scores ( $n = 15$ ) for phonological fluency ( $r_{15} = 0.74$ ,  $p = 0.0027$ ); TMT-A ( $r_{15} = 0.65$ ,  $p = 0.012$ ); TMT-B ( $r_{15} = 0.70$ ,  $p = 0.005$ ); and TMT-B-A ( $r_{15} = 0.62$ ,  $p = 0.018$ ). By contrast, the average CC of salience-visual-DAN was negatively correlated to 3-month postsurgical z-scores but uniquely for semantic fluency ( $r_{15} = -0.67$ ,  $p = 0.0087$ ) (Fig. 5A). Other correlations were nonsignificant (see Fig. 5A and B). Complementary correlation analyses between the preoperative tumor volume and graph theoretical measures were nonsignificant (see Supplementary Fig. 2)

### Discussion

In the present work, we analyzed a rare rsfMRI data set gained from patients with LGGs specifically overwhelming the precuneus—a brain area strategically positioned at the crossroad between several large-scale networks. Our main goal was to characterize both the extent and the nature of the modulations that such lesions might cause in the functional architecture. The critical finding was that various cortical areas remotely situated in relation to the infiltrated structures displayed an rsFC hyperconnectivity profile that can be reasonably interpreted as a compensatory redistribution (i.e., the purpose of which is to mitigate the potential functional consequences of the tumor). As a matter of fact, specific (mainly) hyperconnectivity fin-

**TABLE 3. Connectome MVPA results**

ROI <sub>MVPA</sub> No.	Predominant Region (Harvard-Oxford parcellation)	Cluster Size	MNI Coordinates	Size (p-FDR value)	Peak (p-uncorrected value)
2	Insula (lt)	32	[-42 +10 -8]	0.004834	0.000149
3	Anterior cingulate (rt & lt)	98	[+0 +12 +34]	0.000289	0.000166
4	Precentral & superior frontal gyri (rt)	177	[+28 -4 +72]	0.000002	0.000002
5	Precentral & superior frontal gyri (lt)	395	[-26 -18 +76]	<0.000001	0.000008
6	Postcentral gyri (rt & lt)	111	[-4 -50 +74]	0.000129	0.000024

gerprints involving distinct and distributed functional networks (namely, the salience, DAN, and visual networks) were identified in subsequent network topological analyses as behaviorally relevant, suggesting that such redistributions are physiological markers of functional compensa-

tion. Taken as a whole, these results shed some light on the mechanistic principles that govern lesion-induced neuroplasticity, and add to the emerging literature showing that primary tumors are associated with brainwide changes of functional connectivity.<sup>15</sup> Finally, they indicate that rsFC

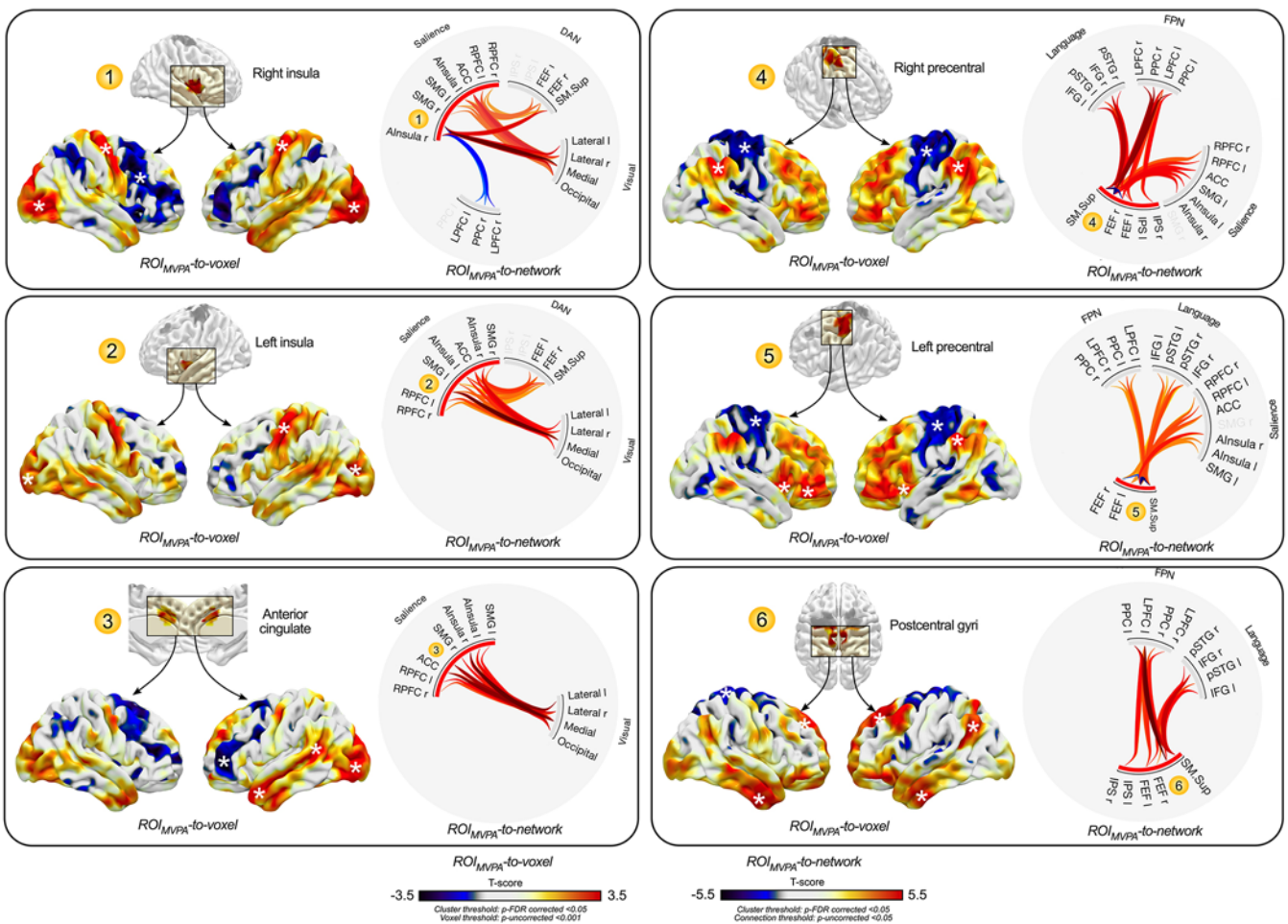


**FIG. 4.** Comparisons of rsFC between patients with precuneal infiltration (n = 17) and healthy controls (n = 17). Significant ROIs resulting from connectome MVPAs (ROI<sub>MVPA</sub>) are labeled from 1 to 6. Each group of illustrations represents the location of the ROI<sub>MVPA</sub> (upper left of each panel), the results of ROI<sub>MVPA</sub>-to-voxel analyses (lower left of each panel, with both left and right hemispheres represented and significant clusters of voxels indicated with a white asterisk), and the results of the ROI<sub>MVPA</sub>-to-network analyses (right side of each panel; only significant connections are presented). Significant ROI<sub>MVPA</sub> and their related MNI central cluster coordinates were as follows: 1) right insular cortex [+42 +12 -2]; 2) left insular cortex [-42 +10 -8]; 3) anterior cingulate cortex (ACC) [+0 +12 +34]; 4) right precentral and superior frontal gyri [+28 -4 +72]; 5) left precentral and superior frontal gyri [-26 -18 +76]; and 6) right and left postcentral gyri [-4 -50 +74]. AInsula = anterior insula; FEF = frontal eye fields; IFG = inferior frontal gyrus; IPS = intraparietal sulcus; LPFC = lateral prefrontal cortex; PPC = posterior parietal cortex; pSTG = posterior superior temporal gyrus; RPFC = rostral prefrontal cortex; SFG = superior frontal gyrus; SM.sup = sensorimotor superior cortex; SMG = supramarginal gyrus. Figure is available in color online only.

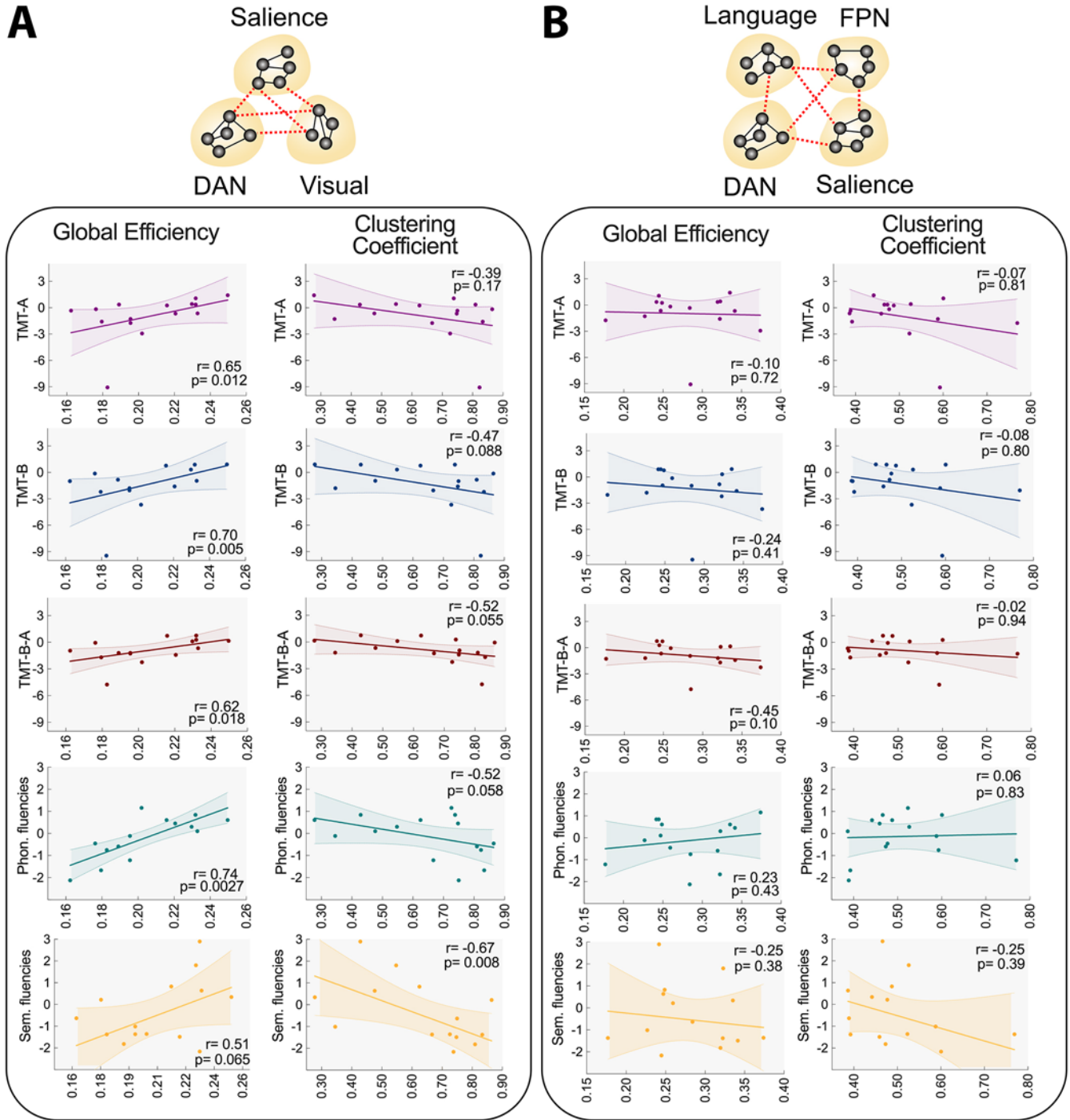


**FIG. 5.** Correlation analyses between GE/CC and postsurgical executive performance in patients with precuneal gliomas. **A:** Saliency-DAN-visual networks. **B:** Language-FPN-DAN-saliency networks. Nonparametric Spearman correlation analyses adjusted for age. Neuropsychological performance results are presented as z-scores. All scores were measured 3 months after precuneal resection. Shaded areas in graphs indicate 95% CI. Phon. = phonological; sem. = semantic. Figure is available in color online only.

modulations should not be uniquely considered as alterations (i.e., negatively predictive of cognitive performance) in the context of brain tumors but also as compensatory ones (i.e., positively predictive of cognitive performance). Increased functional connectivity (commonly referred to as hyperconnectivity) following focal lesional disrupt-

tion has been consistently described in various nontumoral acute and chronic pathological conditions. It has thus been suggested that hyperconnectivity represents an adaptive response to neurological damage and may be a signal for system-level plasticity.<sup>40</sup> Among other neurological diseases, stroke-induced functional connectome reorganiza-

tions and their impact on neurological performance have received particular attention. For instance, sensorimotor recovery has been found to correlate with increased coupling of rsFC between the ipsilesional M1 and contralesional areas.<sup>12</sup> Likewise, increased interhemispheric rsFC<sup>41</sup> or increased ipsilesional FPN coupling<sup>42</sup> have been shown to be predictors of motor recovery.

Potentiating the brain capability to develop neuroplastic compensations through innovative strategies of rehabilitation (e.g., combining neuromodulation and cognitive stimulation) has gained attention over recent decades in various clinical fields, including stroke and neuro-oncology. However, such strategies require an advanced understanding of the compensatory mechanisms activated by the brain in response to neurological lesion at the network system level. In the context of brain tumors, functional redistributions are likely to depend on the tumor's nature and location.<sup>43</sup> Because the precuneus is known to host one of the most complex patterns of functional connectivity in the human brain, our primary working hypothesis was that this structure would be particularly susceptible to inducing widespread modulations of functional connectivity in the event of tumor infiltration. Further studies are needed to ascertain the extent to which these modulations vary as a function of tumor location and, more generally, to model the dynamic interactions between tumor features and behaviorally relevant modulations of functional architecture. This may help in identifying the (modulated) functional fingerprints associated with cognitive compensation versus cognitive decompensation,<sup>44</sup> and thus may help in refining individual surgical preplanning timing for surgical indication and rehabilitation programs. For instance, patients with suboptimal network compensations might be ideal candidates for personalized prehabilitation programs<sup>45</sup> in an attempt to boost neuroplastic modulations before tumor resection—possibly in combination with neuromodulation protocols.

Several notes of caution must be mentioned here. First, because of the extreme rarity of tumors specifically damaging the precuneus, the number of patients included in this study was limited. Hence, to maintain statistical power we did not account for tumor lateralization in rsFC analyses. Second, it was quite surprising that we did not capture significant effects of precuneal infiltration on rsFC within the DMN (ROI-based connectivity analysis) or within the precuneus per se (MVPA). These negative results might be related to a combination of physiological and methodological explanations. It is indeed widely unknown to what extent the infiltrated tissues remain functionally synchronized to the healthy brain, and how the peritumoral tissue might overcompensate intralesional metabolic perturbations, thus compromising the interpretation of ROI-based precuneal connectivity analyses in this pathological context. Third, we were not able to establish correlations between preoperative rsFC modulations and preoperative cognitive scores, because neuropsychological evaluations were not administered systematically before surgery in routine clinical practice at the time of acquisition. Consequently, it should be acknowledged that the modulations of functional connectivity reported in this study might be the result of better cognitive compensation before surgery—

thus representing a possibility for type I error, given that patients with better cognitive status before surgery may present with better cognitive outcomes after surgery.

## Conclusions

Taken together, our results provide evidence that LGGs infiltrating the precuneus promote brainwide modulations of rsFC, and that cortical areas with a high degree of centrality can be to some extent functionally compensated through highly distributed mechanisms. Furthermore, we show that distinct changes in the functional connectome observed in the preoperative setting play a key role in lesion-induced neuroplasticity by supporting the preservation of cognitive performance after neurosurgical excision.

## References

1. Cavanna AE, Trimble MR. The precuneus: a review of its functional anatomy and behavioural correlates. *Brain*. 2006; 129(Pt 3):564-583.
2. Hannawi Y, Lindquist MA, Caffo BS, Sair HI, Stevens RD. Resting brain activity in disorders of consciousness: a systematic review and meta-analysis. *Neurology*. 2015;84(12): 1272-1280.
3. Darby RR, Joutsa J, Burke MJ, Fox MD. Lesion network localization of free will. *Proc Natl Acad Sci U S A*. 2018; 115(42):10792-10797.
4. Silva S, de Pasquale F, Vuillaume C, et al. Disruption of posteromedial large-scale neural communication predicts recovery from coma. *Neurology*. 2015;85(23):2036-2044.
5. Hebscher M, Ibrahim C, Gilboa A. Precuneus stimulation alters the neural dynamics of autobiographical memory retrieval. *Neuroimage*. 2020;210:116575.
6. Herbet G, Lemaitre AL, Moritz-Gasser S, Cochereau J, Duffau H. The antero-dorsal precuneal cortex supports specific aspects of bodily awareness. *Brain*. 2019;142(8):2207-2214.
7. Gusnard DA, Raichle ME. Searching for a baseline: functional imaging and the resting human brain. *Nat Rev Neurosci*. 2001;2(10):685-694.
8. Margulies DS, Vincent JL, Kelly C, et al. Precuneus shares intrinsic functional architecture in humans and monkeys. *Proc Natl Acad Sci U S A*. 2009;106(47):20069-20074.
9. Alstott J, Breakspear M, Hagmann P, Cammoun L, Sporns O. Modeling the impact of lesions in the human brain. *PLoS Comput Biol*. 2009;5(6):e1000408.
10. Gratton C, Nomura EM, Pérez F, D'Esposito M. Focal brain lesions to critical locations cause widespread disruption of the modular organization of the brain. *J Cogn Neurosci*. 2012;24(6):1275-1285.
11. Grefkes C, Fink GR. Reorganization of cerebral networks after stroke: new insights from neuroimaging with connectivity approaches. *Brain*. 2011;134(Pt 5):1264-1276.
12. Wang L, Yu C, Chen H, et al. Dynamic functional reorganization of the motor execution network after stroke. *Brain*. 2010;133(Pt 4):1224-1238.
13. Desmurget M, Bonnetblanc F, Duffau H. Contrasting acute and slow-growing lesions: a new door to brain plasticity. *Brain*. 2007;130(Pt 4):898-914.
14. Lemaitre AL, Herbet G, Ng S, Moritz-Gasser S, Duffau H. Cognitive preservation following awake mapping-based neurosurgery for low-grade gliomas: a longitudinal, within-patient design study. *Neuro Oncol*. 2022;24(5):781-793.
15. Stoecklein VM, Stoecklein S, Galiè F, et al. Resting-state fMRI detects alterations in whole brain connectivity related to tumor biology in glioma patients. *Neuro Oncol*. 2020; 22(9):1388-1398.
16. Almirac F, Deverduin J, Cochereau J, et al. Homotopic redis-

- tribution of functional connectivity in insula-centered diffuse low-grade glioma. *Neuroimage Clin.* 2021;29:102571.
17. Duffau H. Stimulation mapping of white matter tracts to study brain functional connectivity. *Nat Rev Neurol.* 2015; 11(5):255-265.
  18. Harrison JE, Buxton P, Husain M, Wise R. Short test of semantic and phonological fluency: normal performance, validity and test-retest reliability. *Br J Clin Psychol.* 2000; 39(2):181-191.
  19. Tombaugh TN. Trail Making Test A and B: normative data stratified by age and education. *Arch Clin Neuropsychol.* 2004;19(2):203-214.
  20. Godefroy O, GREFEX Study Group. Fonctions exécutives et pathologies neurologiques et psychiatriques: évaluation en pratique clinique. De Boeck Solal; 2008.
  21. Whitfield-Gabrieli S, Nieto-Castanon A. Conn: a functional connectivity toolbox for correlated and anticorrelated brain networks. *Brain Connect.* 2012;2(3):125-141.
  22. Yordanova YN, Cochereau J, Duffau H, Herbet G. Combining resting state functional MRI with intraoperative cortical stimulation to map the mentalizing network. *Neuroimage.* 2019;186:628-636.
  23. Power JD, Mitra A, Laumann TO, Snyder AZ, Schlaggar BL, Petersen SE. Methods to detect, characterize, and remove motion artifact in resting state fMRI. *Neuroimage.* 2014;84: 320-341.
  24. Zhang S, Li CSR. Functional connectivity mapping of the human precuneus by resting state fMRI. *Neuroimage.* 2012; 59(4):3548-3562.
  25. Worsley KJ, Cao J, Paus T, Petrides M, Evans AC. Applications of random field theory to functional connectivity. *Hum Brain Mapp.* 1998;6(5-6):364-367.
  26. Wang Y, Bernanke J, Peterson BS, et al. The association between antidepressant treatment and brain connectivity in two double-blind, placebo-controlled clinical trials: a treatment mechanism study. *Lancet Psychiatry.* 2019;6(8):667-674.
  27. Thompson WH, Thelin EP, Lilja A, Bellander BM, Fransson P. Functional resting-state fMRI connectivity correlates with serum levels of the S100B protein in the acute phase of traumatic brain injury. *Neuroimage Clin.* 2016;12:1004-1012.
  28. Beaty RE, Benedek M, Kaufman SB, Silvia PJ. Default and executive network coupling supports creative idea production. *Sci Rep.* 2015;5(1):10964.
  29. Jafri MJ, Pearlson GD, Stevens M, Calhoun VD. A method for functional network connectivity among spatially independent resting-state components in schizophrenia. *Neuroimage.* 2008;39(4):1666-1681.
  30. Sørensen T. *A Method of Establishing Groups of Equal Amplitude in Plant Sociology Based on Similarity of Species Content and Its Application to Analyses of the Vegetation on Danish Commons.* I kommission hos E. Munksgaard; 1948: 1-34.
  31. Bullmore E, Sporns O. The economy of brain network organization. *Nat Rev Neurosci.* 2012;13(5):336-349.
  32. Hadley JA, Kraguljac NV, White DM, Ver Hoef L, Tabora J, Lahti AC. Change in brain network topology as a function of treatment response in schizophrenia: a longitudinal resting-state fMRI study using graph theory. *NPJ Schizophr.* 2016; 2(1):16014.
  33. Stam CJ, Jones BF, Nolte G, Breakspear M, Scheltens P. Small-world networks and functional connectivity in Alzheimer's disease. *Cereb Cortex.* 2007;17(1):92-99.
  34. Thiebaut de Schotten M, Urbanski M, Duffau H, et al. Direct evidence for a parietal-frontal pathway subserving spatial awareness in humans. *Science.* 2005;309(5744):2226-2228.
  35. Moritz-Gasser S, Herbet G, Duffau H. Mapping the connectivity underlying multimodal (verbal and non-verbal) semantic processing: a brain electrostimulation study. *Neuropsychologia.* 2013;51(10):1814-1822.
  36. Yordanova YN, Duffau H, Herbet G. Neural pathways subserving face-based mentalizing. *Brain Struct Funct.* 2017; 222(7):3087-3105.
  37. Ng S, Herbet G, Lemaitre AL, Moritz-Gasser S, Duffau H. Disrupting self-evaluative processing with electrostimulation mapping during awake brain surgery. *Sci Rep.* 2021;11(1): 9386.
  38. Berger MS, Deliganis AV, Dobbins J, Keles GE. The effect of extent of resection on recurrence in patients with low grade cerebral hemisphere gliomas. *Cancer.* 1994;74(6):1784-1791.
  39. Capelle L, Fontaine D, Mandonnet E, et al. Spontaneous and therapeutic prognostic factors in adult hemispheric World Health Organization Grade II gliomas: a series of 1097 cases: clinical article. *J Neurosurg.* 2013;118(6):1157-1168.
  40. Hillary FG, Roman CA, Venkatesan U, Rajtmajer SM, Bajo R, Castellanos ND. Hyperconnectivity is a fundamental response to neurological disruption. *Neuropsychology.* 2015; 29(1):59-75.
  41. Park CH, Chang WH, Ohn SH, et al. Longitudinal changes of resting-state functional connectivity during motor recovery after stroke. *Stroke.* 2011;42(5):1357-1362.
  42. Schulz R, Buchholz A, Frey BM, et al. Enhanced effective connectivity between primary motor cortex and intraparietal sulcus in well-recovered stroke patients. *Stroke.* 2016;47(2): 482-489.
  43. Voets NL, Parker Jones O, Mars RB, et al. Characterising neural plasticity at the single patient level using connectivity fingerprints. *Neuroimage Clin.* 2019;24:101952.
  44. Siegel JS, Ramsey LE, Snyder AZ, et al. Disruptions of network connectivity predict impairment in multiple behavioral domains after stroke. *Proc Natl Acad Sci U S A.* 2016; 113(30):E4367-E4376.
  45. Rivera-Rivera PA, Rios-Lago M, Sanchez-Casarrubios S, et al. Cortical plasticity catalyzed by prehabilitation enables extensive resection of brain tumors in eloquent areas. *J Neurosurg.* 2017;126(4):1323-1333.

## Disclosures

The authors report no conflict of interest concerning the materials or methods used in this study or the findings specified in this paper.

## Author Contributions

Conception and design: Duffau, Herbet. Acquisition of data: Deverdun, Lemaitre, Moritz-Gasser, Menjot de Champfleury, Duffau, Herbet. Analysis and interpretation of data: Ng, Deverdun, Lemaitre, Giampiccolo, Le Bars, Moritz-Gasser, Duffau, Herbet. Drafting the article: Ng, Herbet. Critically revising the article: Deverdun, Lemaitre, Giampiccolo, Le Bars, Moritz-Gasser, Menjot de Champfleury, Duffau, Herbet. Reviewed submitted version of manuscript: Herbet. Approved the final version of the manuscript on behalf of all authors: Ng. Statistical analysis: Ng, Herbet. Study supervision: Duffau, Herbet.

## Supplemental Information

### Online-Only Content

Supplemental material is available with the online version of the article.

*Supplementary Materials.* <https://thejns.org/doi/suppl/10.3171/2022.9.JNS221723>.

## Correspondence

Sam Ng: Gui de Chauliac Hospital, Montpellier University Medical Center, Montpellier, France. [s-ng@chu-montpellier.fr](mailto:s-ng@chu-montpellier.fr).